ANNALS OF GEOPHYSICS, 68, 2, V221, 2025; doi:10.4401/ag-9185
OPEN ACCESS

AI-Based Multi-Sensor Data Fusion for Near Real-Time Monitoring of Effusive Volcanic Activity: A Case Study of Mount Etna (November 2022 – February 2023) for thermal activity volcano monitoring

Giovanni Salvatore Di Bella[*,1]

[(1)] Istituto Nazionale di Geofisica e Vulcanologia – Osservatorio Etneo, Catania, Italy

Article history: received October 18, 2024; accepted May 16, 2025

Abstract

Earth Observations (EO) play a crucial role in global monitoring of volcanic activity worldwide. Satellite data are continuously acquired by multispectralsensors on board of polar and geostationary satellites orbiting the Earth. EO allows to track ongoing volcanic activity by retrieving eruptive parameters such as the amount of lava erupted in near real time. The heterogeneity of satellite sensors in terms of spatial and temporal resolution requires advanced techniques to automatically estimate volcanic features and combine their outcomes. Here, the potential of integrating Artificial Intelligence (AI) techniques has been demonstrated in processing large amounts of heterogeneous satellite data used to monitor the effusive activity in near real time at Mount Etna from November 2022 to February 2023. Data provided by satellite sensors, including the polar-orbiting Moderate Resolution Imaging Spectroradiometer (MODIS), the Sea and Land Surface Temperature Radiometer (SLSTR), and the Visible Infrared Imaging Radiometer Suite (VIIRS), along with the geostationary Spinning Enhanced Visible and InfraRed Imager (SEVIRI), enable reliable estimates of Volcanic Radiative Power (VRP), areal coverage of lava flows, Time Averaged Discharge Rate (TADR) and the lava volume erupted, and areal coverage of lava flows thanks to Sentinel-2 MSI.

Keywords: Thermal Remote Sensing; Volcano Monitoring; Volcanic Radiative Power; Artificial Intelligence

1. Introduction

Continuous monitoring is essential for assessing the inherent risks associated with natural disasters like volcanic eruptions. In this context, satellite sensors are widely used to monitor the evolution of rapidly changing volcanic phenomena in a timely manner. Nowadays, a variety of satellites orbiting the Earth provide complementary information about volcanic activity (Ramsey et al., 2013; Mia et al., 2017; Torrisi et al., 2023; Corradino et al., 2024).

On one hand, high spatial resolution satellite sensors allow for precise detection of thermal changes, such as those associated with volcanic eruptions. On the other hand, high temporal resolution sensors enable close monitoring of the rapid evolution of volcanic events. This difference in sensor characteristics underscores how the former are essential for detailed analysis of thermal phenomena, while the latter are crucial for real-time tracking of the dynamic development of volcanic activity. Therefore, integrating data from multiple satellites is essential to produce consistent, accurate, and valuable information than any single sensor can provide. By synergistically combining data from diverse satellite sensors with varying temporal, spatial, and spectral characteristics, it is possible to overcome the limitations of individual sensors, offering a comprehensive understanding of volcanic phenomena.

Volcano observatories need automatic techniques to estimate eruptive parameters from satellite data during ongoing volcanic eruptions (Wright et al., 2004; Ganci et al., 2011; Del Negro et al., 2016; Coppola et al., 2016; Marchese et al., 2019). Among these, advanced Artificial Intelligence (AI) approaches, such as machine learning (ML), have been proposed to enhance the accuracy of these estimates, enabling the automation of tasks that cannot easily be described by explicit commands (Corradino et al., 2022; Del Negro et al., 2022; Cariello et al., 2024, Aveni et al., 2024).

This work aims to show the effectiveness of the synergistic integration of advanced cutting-edge Artificial Intelligence techniques and multi-sensor satellite data for near real-time monitoring of effusive volcanic activity. Machine Learning and Deep Learning models already trained and used (references) for a variety of volcano monitoring tasks are here adopted exploiting thermal data from multiple satellite sensors with varying spatial and temporal resolutions. The analytical process follows a well-structured methodological sequence: it begins with the automatic identification of thermal anomalies through volcanic activity recognition techniques (Cariello et al., 2024), implemented via a cascading system that integrates scene classifiers (such as SqueezeNet) with pixel-level segmenters (such as Random Forest), followed by mapping of lava flow extensions (Corradino et al., 2022).

Subsequently, Volcanic Radiative Power (VRP) is estimated using the RSDF algorithm (Di Bella et al., 2024), whose time series allows for detailed tracking of volcanic activity evolution. From this, key eruptive parameters such as the Time-Averaged Discharge Rate (TADR) and the total volume of emitted lava (Del Negro et al., 2016) are automatically derived.

Specifically, the Mount Etna eruption between November 2022 and February 2023 is considered as a study case to show how this approach enabled the accurate detection, classification, and quantification of thermal anomalies, significantly enhancing monitoring precision and ensuring timely identification of critical eruptive dynamics, which are essential for early warning systems.

Overall, the study demonstrates how the integration of AI-based techniques with multi-source satellite observations marks a significant advancement toward automated, efficient operational monitoring systems capable of effectively supporting volcanic risk management.

2. Materials

2.1 Etna: November 2022 - February 2023 effusive eruption

Mount Etna, Europe's highest active volcano in Sicily, constantly shapes the landscape with its eruptions, emitting volcanic ash, pyroclastic material, and lava flows (Harris et al., 2012). Continuously monitored by the Etna Volcano Observatory of Italian National Institute of Geophysics and Volcanology (INGV-OE), Etna's activity ranges from smooth effusive eruptions, outpouring slow basaltic lava flows, to explosive eruptions, presenting numerous hazards such as ash clouds and pyroclastic flows (Marchese et al., 2021; Calvari et al., 2022; Guerrieri et al., 2023). In the summit area of Etna, there are four primary craters named Bocca Nuova, Voragine, Northeast Crater, and Southeast Crater. Originating from the northeastern base of the Southeast Crater at an altitude of around 2,850 meters, a continuous effusive flow commenced on 27 November 2022.

Initially, the lava moved slowly through the desolate Valle del Leone, located on the east flank of Etna, covering several hundred meters before cooling and halting. Subsequently, the eruption was characterized by repeated episodes of lava emission, moving toward the Valle del Bove before cooling and halting. This cyclic pattern persisted for over two months until early February 2023, when the eruption terminated. In contrast to explosive eruptions, characterized by sudden outbursts of ash, gas, and volcanic debris, this effusive episode unfolded gradually, as molten lava flowing steadily onto the surface of Etna.

2.2 Satellite data sources

Different satellite data acquired from Sentinel-2 MSI, MODIS, Sentinel-3 SLSTR, VIIRS, and SEVIRI sensors are utilized to support the monitoring of volcanic activity.

Sentinel-2 MSI is a cutting-edge imaging system managed by the European Space Agency as part of the Copernicus Programme. The Sentinel-2 mission operates two satellites, Sentinel-2A and Sentinel-2B, orbiting 180 degrees apart. This arrangement halves the revisit time from 10 to 5 days for enhanced data availability. With 13 spectral bands spanning visible to shortwave infrared wavelengths and spatial resolutions between 10 to 20 meters, it facilitates detailed monitoring of environmental changes caused by volcanic eruptions.

The Moderate Resolution Imaging Spectroradiometer (MODIS), aboard NASA's Terra and Aqua satellites, delivers global data every 1-2 days across 36 spectral bands ranging from 0.4 µm to 14.4 µm. It features a 12-bit radiometric sensitivity with spatial resolutions of 250 m, 500 m, and 1 km, capturing a 2330-km swath from a 705 km orbit. The optical system employs a rotating double-sided scan mirror and an off-axis telescope, cooled to 83 K for infrared bands. The radiance values are extracted from the MIR (channel 22) and TIR (channel 32) bands. If the brightness temperature exceeds the MIR band's saturation threshold of 328 K, the MIR channel 21 is used instead. Since February 2000, MODIS Level 1 data has been available in geographic projection at 1 km resolution. Data can be accessed via the LAADS web platform.

Sentinel-3 the Sea and Land Surface Temperature Radiometer (SLSTR) is an advanced satellite instrument mounted on both the Sentinel-3A and Sentinel-3B platforms. Its primary function is to precisely measure temperatures of Earth's land and water surfaces. The SLSTR boasts a remarkable precision under 0.2 K and a spatial resolution of 1 km (0.5 km in VIS/SWIR channels). With 9 channels spanning spectral ranges from 0.55 µm to 12.0 µm, it facilitates detection of Earth's surface temperature changes and detailed monitoring of atmospheric parameters across various spectral bands (Seitz et al., 2010). Sentinel-3's S7 (MIR) and S8 bands are used to derive brightness temperature or radiance. Upon surpassing the saturation threshold (312 K and 500 K respectevely), these bands switch to F1 and F2 (Fire Channels). The satellite offers nadir and oblique views, capturing Earth's surface directly below and at an angle, respectively, enriching data with contextual terrain details.

Visible Infrared Imaging Radiometer Suite (VIIRS), another cutting-edge satellite sensor, is deployed on satellites like Suomi NPP and JPSS, providing comprehensive data on Earth's land cover, surface temperatures, and atmospheric parameters. Spatially, it offers high-resolution data acquisition at 375 meters and medium resolution at 750 meters, facilitating detailed surface analysis. VIIRS L1B granules from LAADS-DAAC offer MIR (I4) and TIR (I5) brightness temperature data at 375 m resolution, with saturation points at 367 K and 380 K. Upon saturation, the sensor switches to channels M13 (MIR) and M15 (TIR) at a lower resolution of 750 m to maintain data continuity. Temporally, VIIRS operates with high frequency, often capturing data multiple times a day, enabling frequent monitoring of dynamic events. Spectrally, it spans various bands from visible to infrared wavelengths, allowing comprehensive analysis of land cover, surface temperatures, and atmospheric parameters.

The Spinning Enhanced Visible and Infrared Imager (SEVIRI), onboard EUMETSAT's Meteosat Second Generation satellites, provides data every 15 minutes with spatial resolutions of 3-5 km and 1 km for the High-Resolution Visible channel. It plays a crucial role in weather forecasting, climate monitoring, and environmental research by analyzing parameters like cloud properties and sea surface temperatures. SEVIRI transmits data across 12 spectral channels, focusing on the IR3.9 (MIR) and IR10.8 (TIR) bands. The data is resampled into UTM coordinates on a 12 × 12 km grid, supporting the monitoring of severe weather events, including storms, wildfires, and hurricanes. The saturation threshold for the SEVIRI bands is 335 K.

3. Method

The methodology adopted in this study is grounded in a structured framework that integrates advanced Artificial Intelligence techniques with multi-sensor satellite observations to enable near real-time monitoring of effusive volcanic activity.

A fundamental aspect of this framework is the integration of heterogeneous satellite data from both polar and geostationary platforms, including Sentinel-2 MSI, MODIS, SLSTR, VIIRS, and SEVIRI. The complementary spatial, temporal, and spectral resolutions offered by these sensors allow for a more complete and consistent understanding of the volcanic processes under investigation (McAlpin et al., 2013; Ganci et al., 2023; Di Bella et al., 2024).

Volcanic activity is first identified through the application of Automatic Volcanic Activity Recognition (AVAR) techniques, which employ a cascading model architecture. This system integrates a deep learning scene classifier (SqueezeNet) with a pixel-based segmentation algorithm (Random Forest), both applied to high-resolution Sentinel-2 MSI imagery to detect and validate thermal anomalies (Cariello et al., 2024).

Following the identification of thermal signals, the areal extent of active lava flows is delineated using a supervised Random Forest model trained to recognize thermal anomalies across multiple eruptive events. This allows for precise mapping of lava coverage based on spectral characteristics (Corradino et al., 2022).

To quantify the intensity of the volcanic activity, the Volcanic Radiative Power (VRP) is estimated using the RSDF algorithm, which processes thermal infrared data from MODIS, SLSTR, VIIRS, and SEVIRI sensors (Di Bella et al., 2024). The VRP time series derived from these observations forms the basis for calculating key eruptive parameters, including the Time-Averaged Discharge Rate (TADR) and the total volume of erupted lava.

3.1 Automatic volcanic Activity Recognition

A cascading machine learning algorithm was employed to perform a comprehensive analysis of the effusive events at Mount Etna in November 2022 and February 2023. This approach is designed to accurately detect, classify, and quantify volcanic thermal anomalies using high-resolution Sentinel-2 MSI satellite data (Cariello et al., 2024). The model integrates two main components: a deep learning scene classifier (SqueezeNet), which assigns a global class to each image based on spatial and spectral features, and a pixel-based segmentation model (random forest), which enables precise mapping of thermal anomalies. The cascading architecture improves overall performance by executing the models sequentially and confirming predictions only when a high level of confidence is achieved.

A dedicated dataset was constructed using multispectral imagery acquired by the Sentinel-2 MSI sensor, covering ten active volcanoes between 2016 and 2023. Approximately 1700 images were manually labeled through the combined use of satellite scene inspection and volcanic activity reports from the Smithsonian Institution Global Volcanism Program (https://volcano.si.edu/) and from INGV (https://www.ct.ingv.it).

Each Sentinel-2 MSI scene analyzed by the cascading model is classified into one of four main categories. No Volcanic Activity (NVA) refers to clear-sky scenes with no detectable volcanic thermal activity. Isolated Volcanic Thermal Anomalies (ITA) represent scenes containing localized and spatially confined thermal anomalies, typically associated with summit activity. Extended Volcanic Thermal Anomalies (ETA) indicate scenes with widespread and spatially distributed thermal anomalies. Lastly, Cloudy-Sky Condition (CSC) includes scenes partially or fully obscured by cloud cover, preventing reliable detection of potential thermal signals.

A random split was performed, allocating 60% of the data for training, 10% for validation, and 30% for testing. The test set, comprising previously unseen images, was exclusively used for final model evaluation. Model robustness was assessed by applying the ensemble SqueezeNet model across ten independent runs on the test data.

The high sensitivity of the algorithm also allows for the detection of weak thermal signals, enhancing the accuracy of monitoring, anomaly mapping, and the estimation of the spatial extent of erupted products.

3.2 Areal coverage of active lava

Active lava flows were mapped by processing each newly available Sentinel-2 MSI image through the AI algorithm developed by Corradino et al. (2022), based on a supervised Machine Learning approach. The model consists of a Random Forest classifier composed of 100 decision trees, trained using radiance values from the visible (VIS) to shortwave infrared (SWIR) spectral regions.

The Random Forest (RF) models were trained using six Sentinel-2 MSI images acquired during different volcanic eruptive events at volcanoes such as Etna, Stromboli, Cumbre Vieja, and Pacaya. These images were selected to build a robust and generalized supervised classifier capable of distinguishing thermal anomalies from background features. During the training phase, thermal anomalies were manually identified through expert visual inspection of false-color composites (B12-B11-B5), while background areas were categorized accordingly.

To ensure an unbiased evaluation, the testing phase was performed on completely independent Sentinel-2 MSI scenes not used during training. These included additional eruptive events from the same volcanoes but observed

during different periods, allowing a rigorous assessment of the models' ability to generalize across various volcanic and environmental conditions.

This structure, combined with the ensemble learning method typical of Random Forests, ensures both the effectiveness and reliability of the detection. Overall, the approach enabled accurate and automatic mapping of thermal anomalies associated with the effusive activity of Mount Etna during the 2022-2023 eruption period, capturing a range of signals from low to extreme thermal intensities (Corradino et al., 2022).

3.3 TADR and Volume

A data fusion approach leveraging satellite sensors with medium-to-high temporal resolution enables the estimation and continuous tracking of Time-Averaged Discharge Rate (TADR) and erupted lava volume. These parameters are derived through the estimation of Volcanic Radiative Power (VRP), calculated using the RSDF algorithm (Di Bella et al., 2024). Developed in a local Python environment on a Linux (Ubuntu) system, the RSDF algorithm incorporates a bank of Gabor filters (Ramsey et al., 2023) to enhance the detection of volcanic thermal anomalies (Prayote and Compton, 2006). By combining spectral and spatial information, the algorithm identifies anomalous pixels using Mid-Infrared (MIR) and Thermal Infrared (TIR) bands. The MIR bands are particularly sensitive to high-temperature anomalies, while TIR bands provide detailed surface temperature data. The MIR radiance method assumes a linear relationship between MIR spectral radiance and VRP, and is particularly effective for temperatures above 600 K (Wooster et al., 2003), thus supporting accurate TADR and volume estimations.

The RSDF algorithm enables the detection of hot spots by applying a Gabor filter bank to extract the most significant features from MIR images, effectively enhancing the hottest pixels within the volcanic region. As part of this process, Principal Component Analysis (PCA) is used as a machine learning technique to reduce dimensionality and emphasize the most relevant thermal features (Di Bella et al., 2024).

After applying this algorithm, the "true hotspots" are identified, and VRP (Watt) of each hotspot is calculated following the "MIR radiance method" (Wooster et al., 2003), according to the formula:

$$VRP_{MIR} = \frac{\sigma \cdot \epsilon \cdot A_{pixel}}{a \cdot \epsilon_{MIR}} L_{MIR,h} \Rightarrow VRP_{MIR} = k \cdot \left(L_{MIR} - L_{MIR,bg}\right) \quad (1)$$

where A_{pixel} is the pixel ground sampling area (m^2) and $(L_{MIR} - L_{MIR,bg})$ is the excess of MIR radiance (Corradino et al., 2019, 2022). The background is the average value of the MIR band of the hotspots surrounding the 'true hotspots' detected by the output of the total mask. The constant k is specific for each sensor and depends directly on the parameter a ($k_{MODIS} = 1.89 \times 10^7$ $Wm^{-2}sr^{-1}\mu m^{-1}K^{-4}$, $k_{SLSTR} = 1.70 \times 10^7$ $Wm^{-2}sr^{-1}\mu m^{-1}K^{-4}$, $k_{SEVIRI} = 3.70 \times 10^7$ $Wm^{-2}sr^{-1}\mu m^{-1}K^{-4}$, $k_{VIIRS375} = 2.48 \times 10^7$ $Wm^{-2}sr^{-1}\mu m^{-1}K^{-4}$, and $k_{VIIRS750} = 1.11 \times 10^7$ $Wm^{-2}sr^{-1}\mu m^{-1}K^{-4}$). The parameter k is calculated uniquely for each sensor, following the formula:

$$k = \frac{\sigma \cdot A_{pixel}}{a} \quad (2)$$

The total VRP value for each image acquisition is obtained by summing the VRP value of each individual identified pixel.

The Time-Averaged Discharge Rate (TADR), and lava volume are calculated from the VRP. The TADR refers to the average rate at which volcanic material, such as lava, ash, or gases, is expelled from the volcano over a specific period of time (Coppola et al., 2013):

$$TADR = \frac{VRP}{c_{rad}} \quad (3)$$

Where:

$$c_{rad} = \frac{6.45 * 10^{25}}{X_{SiO_2}^{10.4}} \tag{4}$$

where $X_{SiO_2}^{10.4}$ represents the concentration of silicon dioxide adjusted by a factor of 10.4.

c_{rad} is a parameter dependent on the silica content present in the lava, varying for each volcano. When estimating c_{rad}, it's crucial to consider the significant impact of bulk rheology on lava spreading and cooling. An uncertainty of ±50% in c_{rad} necessitates calculating minimum and maximum TADR values (Ganci et al., 2012; Coppola et al., 2013; Plank et al., 2021). The volume of the lava flow is given by Harris et al., 2012:

$$TADR_{mean} = \frac{TADR_i + TADR_{i-1}}{2} \tag{5}$$

$$Volume_i = TADR_{mean} \cdot \Delta t \tag{6}$$

Various factors contribute to uncertainty, including clouds, volcanic clouds, fires, and satellite viewing angles. Cloud cover can obscure real hotspots, making it difficult to distinguish them from false positives. Additionally, the geometry of the satellite's orbit, with high zenith and azimuth angles, can impede hotspot detection, particularly in deep craters or rugged terrain. Elevated scan angles may also distort thermal anomalies, reducing the accuracy of pixel geolocation.

The saturation temperature represents the maximum limit that satellite sensors can detect before losing the ability to accurately distinguish high temperatures. In volcanic thermal anomaly monitoring, this is a significant issue because eruptions, lava, and pyroclastic flows reach very high temperatures, often exceeding the detection threshold of sensors. Depending on the event type, when sensors saturate, the intensity and extent of thermal anomalies are underestimated, compromising the accuracy of volcanic surveillance and the ability to predict risks in real time. The saturation temperature varies between polar and geostationary sensors.

Geostationary sensors, such as SEVIRI, have a limited detection range and tend to saturate at lower temperatures, compromising the detection of volcanic thermal anomalies. In contrast, polar sensors like MODIS SLSTR and VIIRS provide higher spatial resolution and can detect higher temperatures without saturation, allowing for more accurate measurements, although with less frequent coverage. In the case of periods between two volcanic events, characterized by thermal anomalies with low temperatures, SEVIRI, despite its high temporal resolution, are unable to track and detect insignificant changes in the temperature of the volcanic surface. On the other hand, sensors such as MODIS, SLSTR, and VIIRS, due to their high spatial resolution, are precise and reliable in monitoring low-temperature anomalies.

These challenges introduce uncertainty into the process, complicating the identification of true thermal anomalies and potentially masking hotspots.

	Etna
c_{rad}	2.50×10^8
$c_{rad(max)}$	2.00×10^8
$c_{rad(min)}$	3.60×10^8

Table 1. Values of the parameter c_{rad} for Etna.

4. Results

4.1 Automatic volcanic Activity Recognition

Automatic Volcanic Activity Recognition enables the detection and classification of the various stages of an effusive eruption – from its early onset to its gradual decline – based on the analysis of thermal anomalies in high-resolution satellite imagery.

Figure 1 shows the automatic classification of Sentinel-2 MSI scenes during the effusive activity of Mount Etna between November 2022 and February 2023, divided into four categories: No Volcanic Activity (NVA), Isolated Thermal Anomalies (ITA), Extended Thermal Anomalies (ETA), and Cloudy Sky Condition (CSC). The temporal distribution highlights the ability of the cascading model to track the progression of the eruption, distinguish between different phases of thermal activity, and manage uncertainties related to cloud cover and weak thermal signals.

The performance of the cascading model was evaluated with respect to the case study by calculating standard classification metrics. The analysis yielded an overall accuracy of 89%, confirming the model's strong capability in detecting and classifying volcanic thermal anomalies.

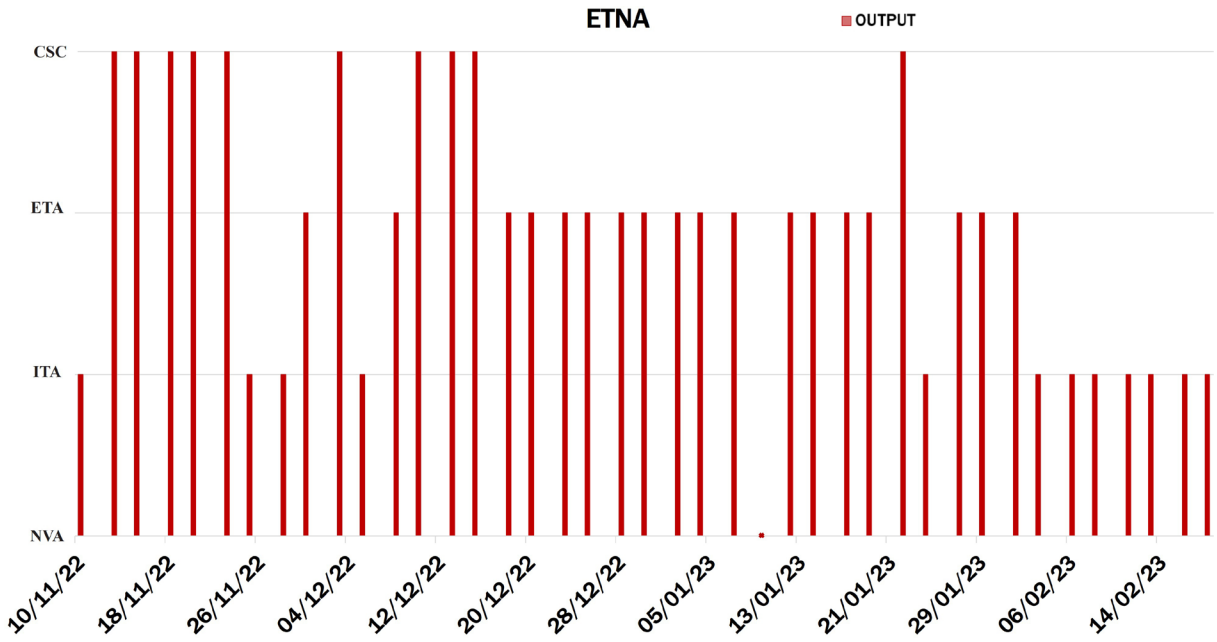

Figure 1. Time Series of Etna activity from 10 November 2022 to 18 February 2023.

4.2 Lava flow areal extension

The Random Forest model (Corradino et al., 2022), showcasing robust generalization capabilities, accurately delineates thermal anomalies during the entire Etna effusive phase. In Fig. 2, a histogram illustrates the values of the areal extension of active lava flows over time. The temporal trend indicates a linear increase in areal coverage until reaching a peak around the midpoint of effusive activity from 28 November 2022 to 2 January 2023. This is followed by a decreasing trend, with a slight rise observed around 27 January 2023, before tapering off. Subsequently, Fig. 3 displays a subset sequence of images captured by the Sentinel-2 sensor over the course of the volcanic event, delineating the active lava field in terms of pixels. The cumulative area covered during the entire event was estimated by overlapping the areas of flow fields calculated for each acquisition. This estimation was derived from the weekly multidisciplinary bulletins compiled by the Etna Volcano Observatory of INGV.

To validate the model's performance, standard classification metrics were computed, resulting in an overall accuracy of 92%, confirming the model's high reliability in detecting and mapping lava flow areas.

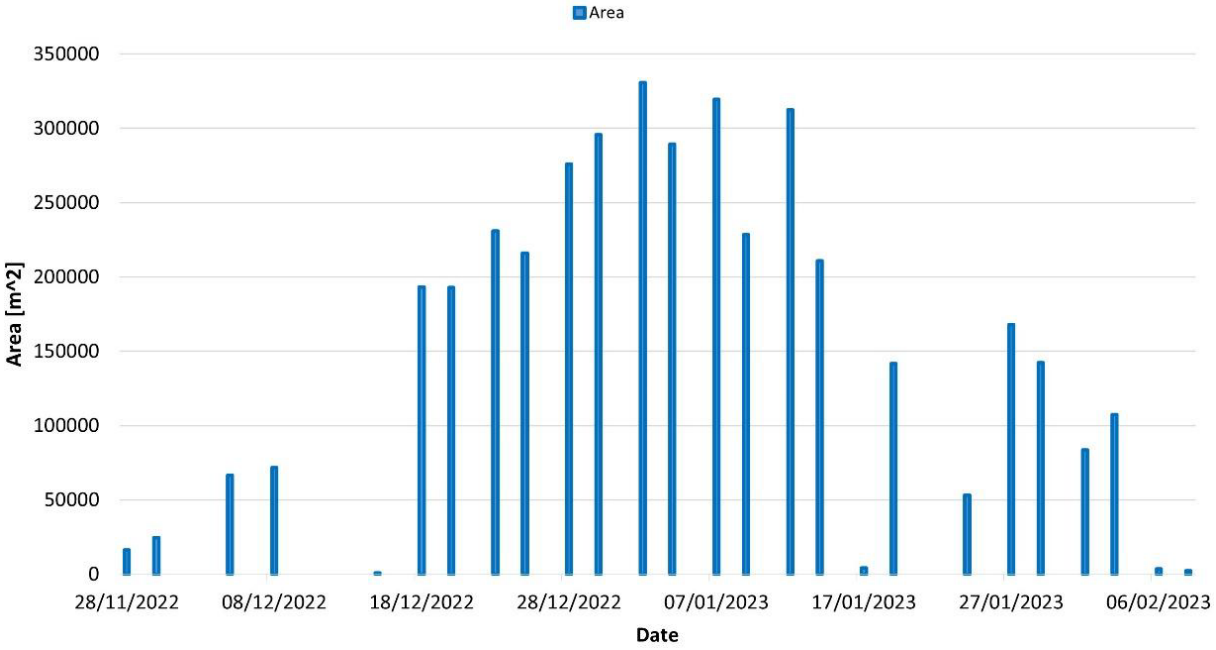

Figure 2. Histogram of areal coverage values of active lava flows over the time obtained using S2 images via GEE.

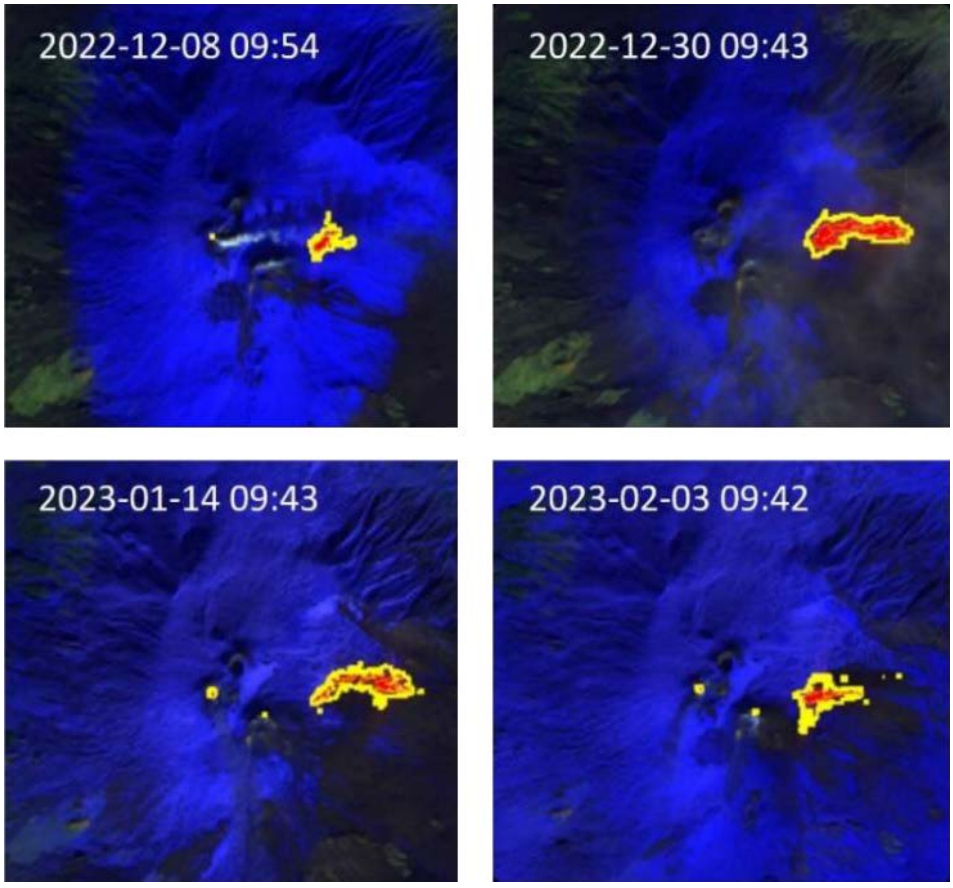

Figure 3. Output of RF model of Lava flow areal extension of Etna, November 2022-February 2023 using Sentinel 2.

4.3 Mean effusion rate and volume

Combining the VRP calculation results using MODIS, SEVIRI, SLSTR, and VIIRS, Fig. 4 shows the temporal trend of VRP values during the period of effusive activity. It is noteworthy that the areas with a high density of points are attributed to the high temporal resolution of SEVIRI, which allows near real-time tracking of the volcanic event's evolution.

The TADR and volume were estimated for the entire duration of effusive activity. Specifically, Fig. 5 depicts the values of effusion rate and cumulative volume during Etna's effusive activity from 28 November 2022 to 10 February 2023. The peak value of the mean effusion rate (red diamonds) is 4.74 m^3/s, occurring on 2 January 2022 at 21:12 UTC. The cumulative mean volume estimated (red curve) is 5,610,958 m^3 on 10 February 2023 at 20:36 UTC.

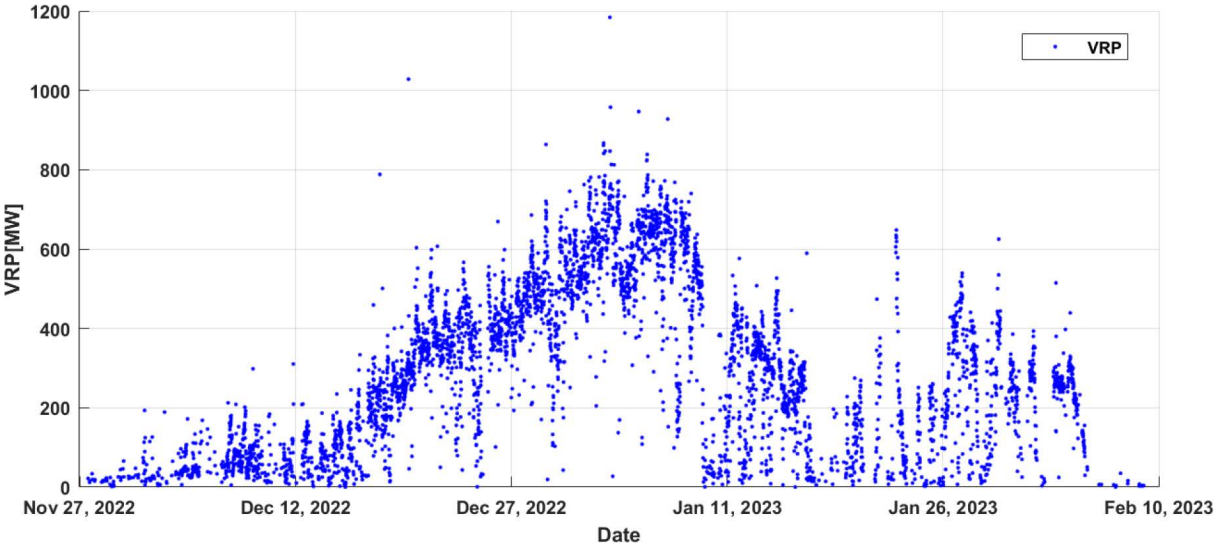

Figure 4. Temporal trend of VRP values derived from the RSDF algorithm for SEVIRI, SLSTR, MODIS, and VIIRS over the period 27 November 2022-10 February 2023 at Mt. Etna.

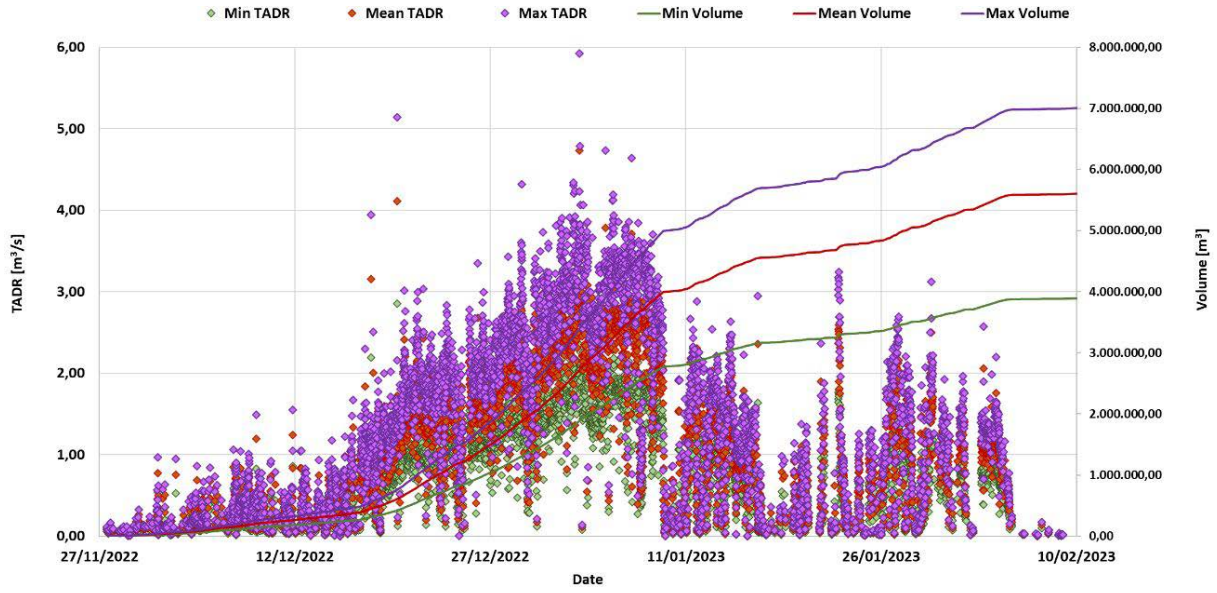

Figure 5. The effusion rate and cumulative volume during the effusive activity of Mount Etna from November 27, 2022, to February 10, 2023, were estimated using satellite data from SEVIRI, SLSTR, MODIS, and VIIRS.

5. Discussion

The effusive activity of Mount Etna between November 2022 and February 2023 was analyzed using a structured and sequential approach inspired by an advanced volcanic monitoring framework, divided into four interconnected phases: Forecasting, Detecting, Tracking, and Quantifying. This operational workflow enabled a progressive interpretation of the event through the integration of Artificial Intelligence techniques and multi-source satellite data.

In the Forecasting phase, the *Automatic Volcanic Activity Recognition* module played a key role in identifying and signaling a potential change in the volcanic state based on thermal anomaly patterns.During the phase preceding the effusive eruption, a clear thermal anomaly was observed in the area of the South-East Crater, clearly detectable through high-resolution satellite data. This anomaly, associated with intense degassing and a progressive increase in surface temperature, showed steady growth in the weeks leading up to the event, intensifying until November 27, 2022, which marks the beginning of the actual effusive activity.

Between November 10 and 27, the automatic recognition model classified several scenes as ITA (Isolated Thermal Anomalies), indicating localized and persistent activity in the summit area of the volcano. However, numerous satellite acquisitions during the same period were classified as CSC (Cloudy Sky Condition) due to frequent cloud cover, which hindered thermal detection. This limited the continuity of observation and the ability to accurately track the evolution of volcanic activity during this initial phase.

The effusive activity began on November 27, 2022, initially detected by the model as an ITA (Isolated Thermal Anomaly), indicating a confined and localized thermal signal. In the days immediately following, the first scene classified as ETA (Extended Thermal Anomaly) appeared, clearly documenting a more widespread effusive activity, with a lava flow emerging and propagating along the northeastern flank of the volcano, within the Valle del Leone. The consistent presence of ETA classifications in the following weeks reflects a sustained period of lava flow activity, closely aligned with the spatial evolution observed during the eruption.

Throughout the analyzed period, frequent transitions between ITA and ETA were observed. These variations may partly reflect real changes in the intensity and spatial distribution of thermal activity, but in some cases, they are attributable to uncertainties in the model's classification. Although the overall accuracy is high (around 95%), such fluctuations often occur in borderline scenes between localized and widespread anomalies, where classification confidence tends to decrease.

A representative example is the case of December 5, 2022, or January 24, 2023, when – despite the effusive activity still being underway – the acquired scene was classified as ITA. This classification did not reflect a real decline in activity but was instead caused by cloud cover that partially or completely obscured the summit area of the volcano. Under these conditions, the sensor detected only a limited portion of the lava flow, leading the model to interpret the anomaly as isolated, despite the broader extent of the phenomenon.

Around January 9, 2023, in the midst of a sequence of scenes classified as ETA, an unexpected NVA (No Volcanic Activity) classification appears. This episode does not indicate a true interruption of the effusive activity, which was still ongoing, but is likely due to model uncertainty resulting from suboptimal observation conditions. Specifically, the presence of thin or partial cloud cover, or a reduced thermal signal in that particular acquisition, may have prevented the model from effectively detecting the anomaly, resulting in a misclassification.

In the final phase of the eruption, from late January to early February 2023, the frequency of ETA classifications progressively decreased, indicating a gradual decline in effusive activity. The last significant thermal anomalies were detected on February 3, after which only isolated or no anomalies were recorded. This trend suggests a reduction in lava output and the eventual cessation of surface activity, marking the natural end of the effusive event. Once an extensive thermal anomaly (ETA) is detected, the system enters the crucial Detecting phase, during which dedicated models for quantitative analysis of volcanic activity are activated. During this phase, the volcano's activity is continuously monitored through thermal data from various satellite sensors, enabling the prompt identification of potentially hazardous volcanic phenomena, such as lava flows, volcanic plumes, or pyroclastic deposits.

The ETA classification serves as an activation signal for the processing of more detailed eruptive parameters. Specifically, a Random Forest-based segmentation model has been applied to high-resolution Sentinel-2 MSI images to accurately map the area affected by active lava flows, providing fundamental geometric information such as surface area and flow length. Simultaneously, the RSDF algorithm has been applied to data from medium and high-frequency thermal sensors (MODIS, SLSTR, SEVIRI, VIIRS) to estimate, in near-real-time, the Volcanic

Radiative Power (VRP). The VRP, represented as a time series, describes the evolution of the radiative flux emitted by the volcanic surface and is a key parameter for evaluating the intensity and dynamics of effusive activity.

In the subsequent Tracking phase, time series of Volcanic Radiative Power (VRP) provided a continuous and detailed view of the thermal energy emitted by lava flows, allowing for near-real-time monitoring of the evolution of effusive activity.

The analysis of the evolution of Etna's effusive activity, obtained by combining data from various satellite sensors and techniques based on artificial intelligence algorithms, has made it possible to reconstruct in detail the temporal trend of the Time-Averaged Discharge Rate (TADR), cumulative volume, and the surface area covered by lava flows (Fig. 6). The eruption follows a typical pattern previously described in the literature (Del Negro et al., 2013; 2020), consisting of two main phases: a rising phase, during which the emitted volume increases rapidly until reaching a peak, followed by a decreasing phase that continues until the end of the event. In this specific case, a significant increase in activity is evident starting from December 17, 2022, with a peak between December 29 and January 2, 2023, followed by a sharp decrease in the TADR.

The comparison between the mean TADR trend, calculated on a daily basis and the areal extension of active lava flows estimated from Sentinel-2 MSI data, shows a good agreement between the two indicators. Although Sentinel-2 provides data with lower temporal resolution, its high spatial resolution allows for an effective representation of the lava flow evolution in terms of surface area. The similarity in the two curves confirms the robustness of the method used to integrate observations from different sources, with complementary characteristics, for volcanic monitoring purposes.

Discrepancies observed in some points of the figure – where an increase in TADR does not correspond to a surface area expansion – can be attributed to both data acquisition uncertainties, such as suboptimal atmospheric conditions or classification errors, and to physical phenomena such as lava flow superposition. In these cases, new lava is deposited over pre-existing flows, increasing the total volume without altering the visible surface extension, which thus appears unchanged. Moreover, the analysis of high-frequency variations in the TADR signal highlights a pulsating behavior of effusive activity throughout the entire eruptive period. This variability likely reflects internal dynamics of the magmatic plumbing system, functioning similarly to a valve, where magma accumulates and is subsequently released in an intermittent fashion.

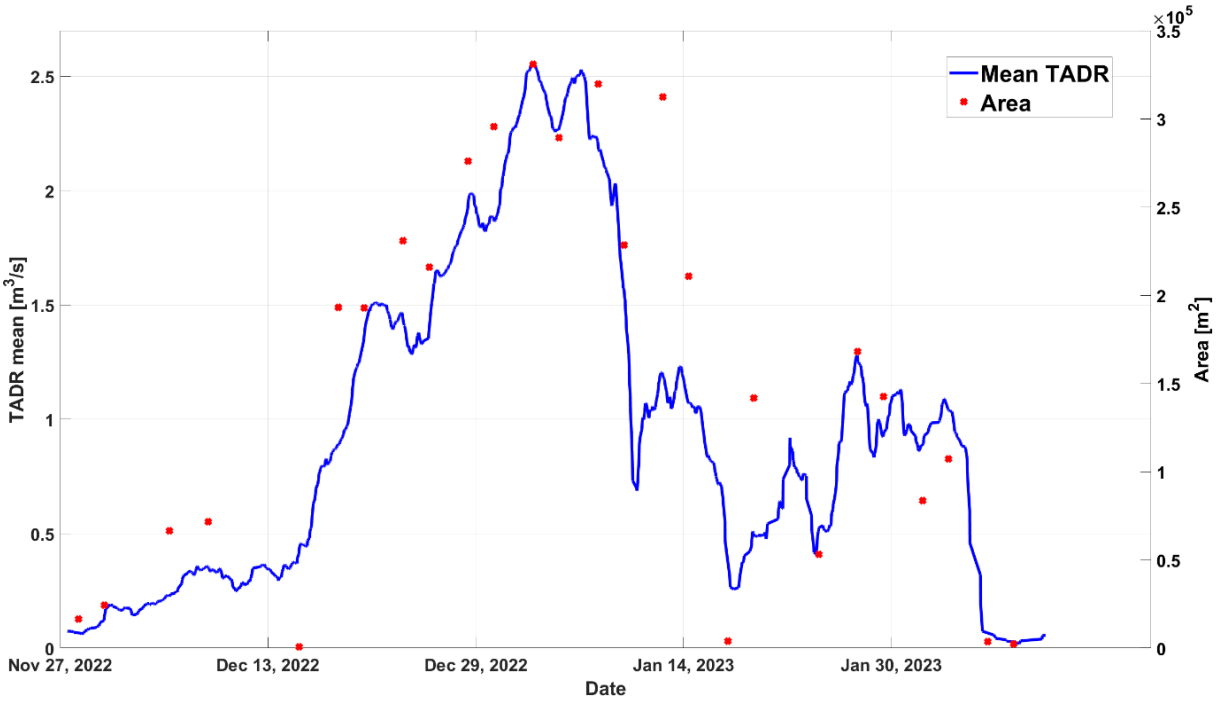

Figure 6. The mean TADR (1-day moving average) estimated using satellite data from SEVIRI, SLSTR, MODIS, and VIIRS. areal extension of active lava flows estimated using S2, during the effusive activity of Mount Etna from November 27, 2022, to February 10, 2023.

The final phase of Quantifying integrated all the results from the previous phases to provide a comprehensive quantitative assessment of the effusive event. Starting from the sequence of Sentinel-2 MSI images acquired between November 28, 2022, and February 3, 2023, the map of the cumulative lava field was reconstructed, which allowed for the estimation of a total surface area of 0.98 km² and an overall flow length of 1920 meters.

As expected, the areal extension of the active lava flow reaches a peak on the 2 January 2023. Meaning that thickness has been generally kept constant, the ratio between volume and area. Thus, we can estimate that the average thickness value of the final lava flow is:

$$averaged\ thickness = \frac{Cumulative\ Volume}{Cumulative\ Area} = 5.6\ \text{m} \tag{7}$$

These results highlight the value of an integrated and automated approach based on AI and satellite observations for the operational monitoring of effusive eruptions.

6. Conclusion

This study demonstrates the effectiveness of an AI-based multi-sensor integration strategy for near real-time monitoring of effusive volcanic activity, specifically applied to the Mount Etna eruption from November 2022 to February 2023. By combining thermal data from multiple satellite sensors with varying spatial and temporal resolutions and applying advanced machine learning techniques, volcanic thermal anomalies can be detected, classified, and quantified with high accuracy. This approach improved monitoring precision and enabled timely identification of key eruption dynamics, essential for early warning systems and hazard mitigation.

The cascading classification model effectively recognized different eruption phases using Sentinel-2 MSI imagery, differentiating between isolated, extended, and cloud-obscured anomalies, despite challenges like cloud cover. The integration of a Random Forest-based model for lava flow mapping provided accurate estimates of active lava field areas, offering essential insights into the spatial evolution of the eruption.

Additionally, the RSDF algorithm applied to medium and high-frequency thermal sensors (MODIS, SLSTR, SEVIRI, VIIRS) enabled the estimation of Volcanic Radiative Power (VRP), crucial for assessing effusive activity intensity. This time series helped derive critical parameters like the Time-Averaged Discharge Rate (TADR) and cumulative lava volume, which were used to calculate average lava thickness, reinforcing the value of combining spatial, thermal, and temporal data.

The temporal evolution of these parameters revealed a typical two-phase eruption trend: rapid growth followed by decline, consistent with known eruption models. The simultaneous analysis of TADR and lava flow area helped capture the eruption's dynamics and allowed for a comprehensive understanding of lava volume and surface area changes over time.

In conclusion, this study emphasizes the importance of refining real-time observation algorithms to enhance volcanic monitoring accuracy and reliability. The use of AI significantly improves understanding and forecasting of volcanic processes, while integrating data from various sensors compensates for individual sensor limitations. Looking ahead, techniques like super-resolution hold promise for enhancing spatial resolution, particularly for geostationary satellites, which would further refine volcanic activity monitoring.

Acknowledgements. This work was developed within the framework of the Laboratory of Technologies for Volcanology (TechnoLab) at the Istituto Nazionale di Geofisica e Vulcanologia (INGV) in Catania (Italy). This research was funded by the Athos research program (INGV OB.FU. 0867.010), by the 2019 strategic project first – forecasting eruptive activity at Stromboli volcano: timing, eruptive style, size, intensity, and duration – of the INGV Volcanoes Department (DELIBERA n. 144/2020), and by Project INGV Pianeta Dinamico VT_ORME 2023-2025 (INGV OB.FU. 1020.010).

References

Aveni, S., M. Laiolo, A. Campus, F. Massimetti et al. (2024). TIRVolcH: Thermal Infrared Recognition of Volcanic Hotspots. A single band TIR-based algorithm to detect low-to-high thermal anomalies in volcanic regions, Remote Sens. Environ., 315, 114388, doi:10.1016/j.rse.2024.114388.

Calvari, S. and G. Nunnari (2022). Comparison between automated and manual detection of lava fountains from fixed monitoring thermalcameras at Etna volcano, Italy, Remote Sens., 14, 2392, doi:10.3390/rs14102392.

Cariello, S., C. Corradino, F. Torrisi and C. Del Negro (2024). Cascading Machine Learning to Monitor Volcanic Thermal Activity Using Orbital Infrared Data: From Detection to Quantitative Evaluation, Remote Sens., 16, 1, doi:10.3390/rs16010171.

Coppola, D., M. Laiolo, C. Cigolini, D. Delle Donne et al. (2016). Enhanced volcanic hot-spot detection using MODIS IR data: Results from the MIROVA system, Geol. Soc. Spec. Publ., 2016, 426, 181-205, doi:10.1144/SP426.5.

Coppola, D., M. Laiolo, D. Piscopo and C. Cigolini (2013). Rheological control on the radiant density of active lava flows and domes, J. Volcan. Geotherm. Res., 249, 39-48, doi:10.1016/j.jvolgeores.2012.09.005.

Corradino, C., G. Ganci, G. Bilotta, A. Cappello et al. (2019). Smart Decision Support Systems for Volcanic Applications, Energies, 12, 1216, doi:10.3390/en12071216.

Corradino, C., E. Amato, F. Torrisi, C. Corradino et al. (2022). Data-Driven Random Forest Models for Detecting Volcanic Hot Spots in Sentinel-2 MSI Images, Remote Sens., 14, 17, doi:10.3390/rs14174370.

Corradino, C., A. B. Malaguti, M. S. Ramsey and C. Del Negro (2024). Quantitative Assessment of Volcanic Thermal Activity from Space Using an Isolation Forest Machine Learning Algorithm, Remote Sens., 16, 2001, doi:10.3390/rs16112001.

Del Negro, C., A. Cappello, M. Neri, G. Bilotta et al. (2013). Lava flow hazards at Mount Etna: constraints imposed by eruptive history and numerical simulations, Sci. Rep., 3, 3493, doi:10.1038/srep03493.

Del Negro, C., A. Cappello and G. Ganci (2016). Quantifying lava flow hazards in response to effusive eruption, Geol. Soc. Am. Bull., 28, 752-763, doi:10.1130/B31364.1.

Del Negro, C., A. Cappello and G. Ganci (2016). Quantifying lava flow hazards in response to effusive eruption, Geol. Soc. Am. Bull., 128, 5-6, 752-763, doi:10.1130/B31364.1.

Del Negro, C., A. Cappello, G. Bilotta, G. Ganci et al. (2020). Living at the Edge of an Active Volcano: Risk from Lava Flows on Mt Etna, Geol. Soc. Am. Bull., 132, 7-8, 1615-1625, doi:10.1130/B35290.1.

Del Negro, C., E. Amato, F. Torrisi, C. Corradino et al. (2022). Support Vector Machine for volcano hazard monitoring from space at Mount Etna, in Proceedings of the 2022 IEEE 21st Mediterranean Electrotechnical Conference (MELECON), Palermo, Italy, 14-16 June 2022, 627-631, doi:10.1109/MELECON53508.2022.9842942.

Ganci, G., A. Cappello and M. Neri (2023). Data Fusion for Satellite-Derived Earth Surface: The 2021 Topographic Map of Etna Volcano, Remote Sens., 15, 198, doi:10.3390/rs15010198.

Ganci, G., A. Vicari, A. Cappello and C. Del Negro (2012). An emergent strategy for volcano hazard assessment: From thermal satellite monitoring to lava flow modeling, Remote Sens. Environ., 119, 197-207, doi:10.1016/j.rse.2011.12.021.

Ganci, G., A. Vicari and C. Del Negro (2011). The HOTSAT Volcano Monitoring System Based on a Combined Use of SEVIRI and MODIS Multispectral Data, Ann. Geophys., 54, 5338, doi:10.4401/ag-5338.

Guerrieri, L., S. Corradini, N. Theys, D. Stelitano et al. (2023). Volcanic Clouds Characterization of the 2020-2022 Sequence of Mt. Etna Lava Fountains Using MSG-SEVIRI and Products' Cross-Comparison., Remote Sens., 15, 2055, doi:10.3390/rs15082055.

Harris, A. J. L., A. Steffke, S. Calvari and L. Spampinato (2011). Thirty years of satellite-derived lava discharge rates at Etna: Implications forsteady volumetric output, J. Geophys. Res. Solid Earth, 116, B8, doi:10.1029/2011JB008237.

Marchese, F., C. Filizzola, T. Lacava, A. Falconieri et al. (2021). Mt. Etna paroxysms of February-April 2021 monitored and quantified through a multi-platform satellite observing system, Remote Sens., 13, 3074, doi:10.3390/rs13163074.

Marchese, F., N. Genzano, M. Neri, A. Falconieri et al. (2019). A multi-channel algorithm for mapping volcanic thermal anomalies by means of Sentinel-2 MSI and Landsat-8 OLI data, Remote Sens., 11, 2876, doi:10.3390/rs11232876.

McAlpin, D. and F. J. Meyer (2013). Multi-sensor data fusion for remote sensing of post-eruptive deformation and depositional features at Redoubt Volcano, J. Volcanol. Geotherm. Res., 259, 414-423, doi:10.1016/j.jvolgeores.2012.08.006.

Mia, M. B., Y. Fujimitsu and J. Nishijima (2017). Thermal activity monitoring of an active volcano using Landsat 8/OLI-TIRS sensor images: A case study at the Aso volcanic area in southwest Japan, Geosci., 7, 118, doi:10.3390/geosciences7040118.

Plank, S., F. Massimetti, A. Soldati, K. U. Hess et al. (2021). Estimates of lava discharge rate of 2018 Kīlauea Volcano, Hawai'i eruption using multi-sensor satellite and laboratory measurements, Int. J. Remote Sens., 42, 4, 1492-1511, doi:10.1080/01431161.2020.1834165.

Prayote, A. and P. Compton (2006). Detecting Anomalies and Intruders in AI06, Hobart, doi:10.1007/11941439_127.

Ramsey, M., C. Corradino, J. Thompson and T. N. Leggett (2023). Statistical retrieval of volcanic activity in long time series orbital data: Implications for forecasting future activity, Remote Sens. Environ., 295, 113704, doi:10.1016/j.rse.2023.113704.

Ramsey, M. S. and A. J. L. Harris (2013). Volcanology 2020: How will thermal remote sensing of volcanic surface activity evolve over the next decade?, J. Volcanol. Geotherm. Res., 249, 217-233, doi:10.1016/j.jvolgeores.2012.05.011.

Seitz, B., C. Mavrocordatos, H. Rebhan, J. Nieke et al. (2010). The sentinel-3 mission overview, International Geoscience and Remote Sensing Symposium (IGARSS), Honolulu, HI, USA, 4208-4211, doi:10.1109/IGARSS.2010.5650772.

Torrisi, F., E. Amato, C. Corradino and C. Del Negro (2023). The FastVRP automatic platform for the thermal monitoring of volcanicactivity using VIIRS and SLSTR sensors: FastFRP to monitor volcanic radiative power, Ann. Geophys., 65, 1, doi:10.4401/ag-8823.

Wooster, M. J., B. Zhukov and D. Oertel (2003). Fire radiative energy for quantitative study of biomass burning: Derivation from the BIRD experimental satellite and comparison to MODIS fire products, Remote Sens. Environ., 86, 83-107, doi:10.1016/S0034-4257(03)00070-1.

Wright, R., L. Flynn, H. Garbeil, A. Harris et al. (2004). MODVOLC: Near-real-time thermal monitoring of global volcanism, J. Volcanol. Geotherm Res., 135, 29-49, doi:10.1016/j.jvolgeores.2003.12.008.

***CORRESPONDING AUTHOR: Giovanni Salvatore DI BELLA**,
Istituto Nazionale di Geofisica e Vulcanologia – Osservatorio Etneo, Catania, Italy
e-mail: giovanni.dibella@ingv.it